

Accessing new magnetic regimes by tuning the ligand spin-orbit coupling in van der Waals magnets

Thomas A. Tartaglia,¹ Joseph N. Tang,¹ Jose L. Lado,²
Faranak Bahrami,¹ Mykola Abramchuk,¹ Gregory T. McCandless,³
Meaghan C. Doyle,¹ Kenneth S. Burch,¹ Ying Ran,¹
Julia Y. Chan,³ Fazel Tafti,^{1†}

¹Department of Physics, Boston College, Chestnut Hill, MA 02467, USA

²Department of Applied Physics, Aalto University, Espoo, Finland

³Department of Chemistry and Biochemistry, University of Texas at Dallas, Richardson, TX 75080, USA

†fazel.tafti@bc.edu

One Sentence Summary: New magnetic regimes and phenomena are revealed by tuning the competition between two types of spin-orbit coupling.

Van der Waals (VdW) materials have opened new directions in the study of low dimensional magnetism. A largely unexplored arena is the intrinsic tuning of VdW magnets toward new ground-states. The chromium trihalides provided the first such example with a change of inter-layer magnetic coupling emerging upon exfoliation. Here, we take a different approach to engineer new ground-states, not by exfoliation, but by tuning the spin-orbit coupling (SOC) of the non-magnetic ligand atoms (Cl,Br,I). We synthesize a three-halide series, $\text{CrCl}_{3-x-y}\text{Br}_x\text{I}_y$, and map their magnetic properties as a function of Cl, Br, and I content. The resulting triangular phase diagrams unveil a frustrated regime near CrCl_3 . First-principles calculations confirm that the frustration is driven by a competition between the chromium and halide SOC. Furthermore, we reveal a field-induced change of inter-layer coupling in the bulk of $\text{CrCl}_{3-x-y}\text{Br}_x\text{I}_y$ crystals at the same field as in the exfoliation experiments.

Introduction

Spin-orbit coupling (SOC) is an essential ingredient of exotic magnetic phenomena. For example, the Dzyaloshinski-Moriya interaction that leads to the formation of Skyrmions originates from a combination of SOC and broken inversion symmetry (*1*). The Kitaev interaction that leads to long-range entanglement in quantum spin liquids is also rooted in SOC (*2, 3*). Ferromagnetic (FM) ordering in single atomic layers of 2D magnets is a result of SOC and magnetic anisotropy according to the Mermin-Wagner theorem (*4–8*). Despite the fundamental importance of SOC, little has been done to tune this interaction beyond the single-ion level. In this manuscript, we generate the entire magnetic phase diagram of chromium trihalides by tuning the ligand SOC. This is done by varying the ratio of the non-magnetic ligand atoms (Cl, Br, I) in $\text{CrCl}_{3-x-y}\text{Br}_x\text{I}_y$ without affecting the magnetic atom (Cr).

Our experiments were motivated by the following model Hamiltonian recently proposed for chromium trihalides (*9–12*).

$$\mathcal{H} = -J \sum_{\langle i,j \rangle} \mathbf{S}_i \cdot \mathbf{S}_j - D \sum_i (S_i^z)^2 - \lambda \sum_{\langle i,j \rangle} S_i^z S_j^z + H_{\text{frust.}} \quad (1)$$

It describes the Cr^{3+} ions with $S = 3/2$ and isotropic Heisenberg coupling (J) on a honeycomb lattice (Fig. 1). Magnetic anisotropy is controlled by the single-ion anisotropy (D) and the anisotropic exchange (λ). The main contribution to D is from the SOC of Cr. The main contribution to λ is from the SOC of the heavy ligands (Br and I), but Cr and Cl could also contribute to a lesser extent. Other interactions that promote magnetic frustration, such as the Kitaev or dipolar interactions, are contained in $H_{\text{frust.}}$. The in-plane anisotropy in CrCl_3 (*13*) implies $D < 0$ and the out-of-plane anisotropy in CrI_3 (*14*) implies $\lambda > 0$. Thus, a competition is built into Eq. 1 that could drive the system into a frustrated regime due to $H_{\text{frust.}}$ when D and λ acquire comparable magnitudes (with opposite signs). The atomic SOC values in Cr, Cl, Br, and I are 90, 40, 220, and 580 meV, respectively (*15*). From here, we expect to see the effect of $H_{\text{frust.}}$ near CrCl_3 where D and λ could cancel each other, but not in CrBr_3 or CrI_3 where a strong λ leads to a dominant out-of-plane FM order. To search for such a frustrated regime, we

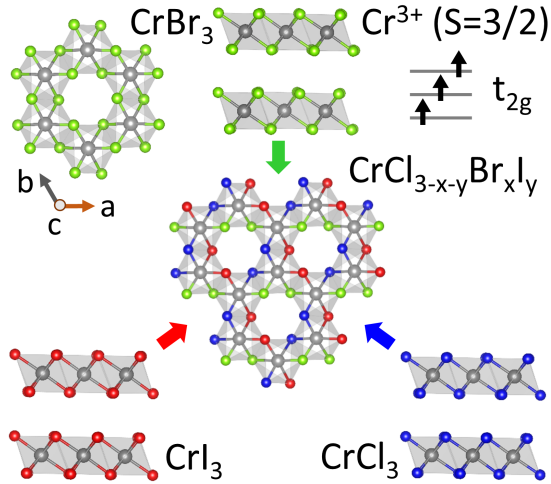


Figure 1: The $\text{CrCl}_{3-x-y}\text{Br}_x\text{I}_y$ alloys with a honeycomb layered structure were synthesized by a CVT process from mixtures of CrCl_3 , CrBr_3 , and CrI_3 in appropriate ratios. The gray, blue, green, and red spheres represent Cr^{3+} , Cl^- , Br^- , and I^- , respectively. Cr^{3+} is a spin $3/2$ ion with three electrons in the t_{2g} manifold.

grew a series of three-halide crystals $\text{CrCl}_{3-x-y}\text{Br}_x\text{I}_y$ and mapped their Curie temperature (T_C), Weiss temperature (Θ_W), and frustration index ($f = \Theta_W/T_C$), as a function of Cl, Br, and I content. As expected, our experiments revealed a frustrated regime near CrCl_3 with maximum f in $\text{CrCl}_{2.55}\text{Br}_{0.45}$.

In addition to finding a frustrated regime, we reveal a field-induced change of inter-layer coupling from antiferromagnetic (AF) to ferromagnetic (FM) in the bulk $\text{CrCl}_{3-x-y}\text{Br}_x\text{I}_y$ crystals. So far, such metamagnetic transition has been observed only in exfoliation experiments due to the monoclinic stacking of two atomic layers (bilayer) of CrI_3 (4, 5, 16) and CrBr_3 (17). We show, for the first time, that a similar metamagnetic transition can be engineered in the bulk of $\text{CrCl}_{3-x-y}\text{Br}_x\text{I}_y$ intrinsically.

Results

VdW Alloys

Single crystals of $\text{CrCl}_{3-x-y}\text{Br}_x\text{I}_y$ were grown via a chemical vapor transport (CVT) technique from the parent compounds CrCl_3 , CrBr_3 , and CrI_3 (see Fig. 1 and Methods). We refer to these single-phase solid-solutions as *VdW alloys*. The layered structure of the VdW alloys is illustrated in Fig. 1. Each layer is a 2D honeycomb lattice made of edge-sharing octahedra around the Cr^{3+} ions. There are three electrons in the t_{2g} levels of Cr^{3+} , giving rise to $S = 3/2$ regardless of the halide ratios in $\text{CrCl}_{3-x-y}\text{Br}_x\text{I}_y$ (Fig. 1). We point out that mixtures of Cl/Br ($\text{CrCl}_{3-x}\text{Br}_x$) and Br/I ($\text{CrBr}_y\text{I}_{3-y}$) have been reported before (18), but the three-halide series, the frustrated regime, and the bulk metamagnetic transition are presented here for the first time. We could not grow crystals of $\text{CrCl}_x\text{I}_{3-x}$ due to the significant size difference between Cl and I. A black contour in the phase diagrams of Figs. 2 and 4 marks the approximate region of insolubility. Therefore, the intermediate size of Br seems to be crucial in the formation of $\text{CrCl}_{3-x-y}\text{Br}_x\text{I}_y$.

Triangular Phase Diagrams

The phase diagrams of Fig. 2 show that both T_C and Θ_W are controlled continuously by tuning the halide composition. This expands the list of available VdW magnets from the parent compounds, CrCl_3 , CrBr_3 , and CrI_3 , to a continuum of compositions $\text{CrCl}_{3-x-y}\text{Br}_x\text{I}_y$ with tunable magnetic properties. Both T_C and Θ_W acquire minimum values near CrCl_3 , intermediate values near CrBr_3 , and maximum values near CrI_3 . We used a linear interpolation to produce the color maps in Fig. 2 based on the magnetic susceptibility data from 27 samples. For each sample, the data were fitted to a Curie-Weiss (CW) expression, $\chi = \chi_0 + C/(T - \Theta_W)$, where χ_0 is a temperature-independent contribution to susceptibility, C is the Curie constant related to the effective magnetic moment ($\mu = \mu_B\sqrt{8C}$), and Θ_W is the Weiss temperature related to the exchange coupling ($J = k_B\Theta_W/2S(S + 1)$).

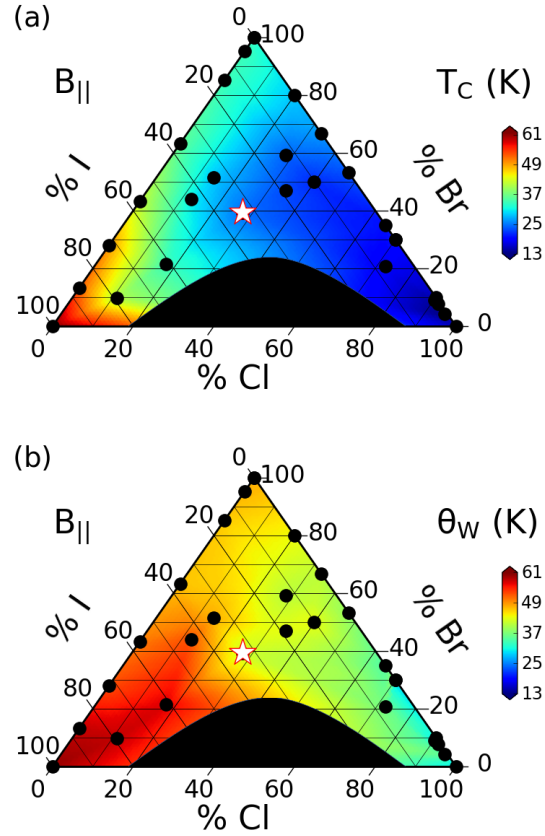


Figure 2: (a) Triangular phase diagram of T_C as a function of composition in $\text{CrCl}_{3-x-y}\text{Br}_x\text{I}_y$ with field in the plane (B_{\parallel}). The star symbol near the center is a composition with 27% Cl (bottom axis), 40% Br (right axis), and 33% I (left axis), corresponding to $\text{Cr}(\text{Cl}_{0.27}\text{Br}_{0.40}\text{I}_{0.33})_3 = \text{CrCl}_{0.8}\text{Br}_{1.2}\text{I}_{1.0}$. (b) Triangular phase diagram of Θ_W . The color maps are produced by a linear interpolation between the 27 discrete data points, each represented by a black circle. Some of the two-halide samples are the same as in ref. (18).

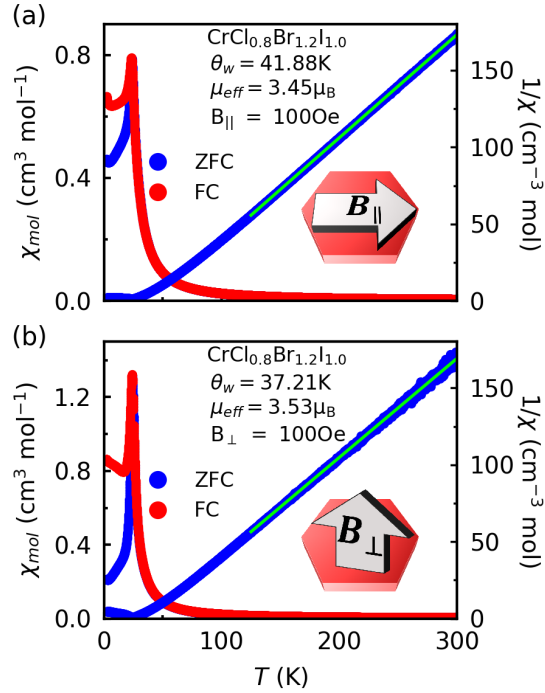


Figure 3: Representative Curie-Weiss analyses on $\text{CrCl}_{0.8}\text{Br}_{1.2}\text{I}_{1.0}$ measured with field (a) parallel and (b) perpendicular to the honeycomb layers. The observation of a single sharp peak rules out disorder or chemical inhomogeneity (see also Fig. S3). Both the zero-field cooled (ZFC, blue) and field-cooled (FC, red) data are presented. Solid green lines show the Curie-Weiss fit to the ZFC data. The Weiss temperature Θ_W and effective moment μ_{eff} are comparable between the B_{\parallel} and B_{\perp} configurations.

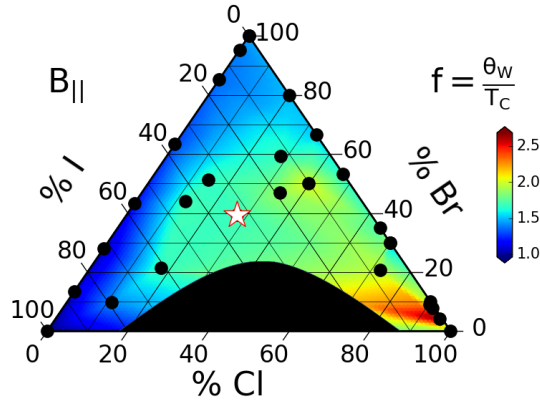


Figure 4: Frustration index ($f = \Theta_W/T_C$) as a function of composition in $\text{CrCl}_{3-x-y}\text{Br}_x\text{I}_y$. This map is only a qualitative measure of frustration, especially since the f -index was originally proposed for isotropic (not anisotropic) magnets (19).

A representative CW analysis is shown in Figs. 3(a) and (b) for $\text{CrCl}_{0.8}\text{Br}_{1.2}\text{I}_{1.0}$, the sample marked as a star near the center of the phase diagrams in Fig. 2. The magnetization of all samples were measured with the magnetic field both parallel (B_{\parallel}) and perpendicular (B_{\perp}) to the honeycomb planes. The effective moment evaluated by the CW analysis in all samples is close to $3.87 \mu_B$ corresponding to Cr^{3+} (Fig. 2 and S3). The transition temperature for each sample can be determined from the peak in either $\chi(T)$ or $d\chi(T)/dT$. Although the results are comparable, we choose the latter criterion because it yields less uncertainty (Supplementary Material). The triangular phase diagrams of Fig. 2 are constructed from the CW analysis on all samples in the B_{\parallel} configuration. The results for B_{\perp} configuration are similar and presented in the Supplementary Material (SM).

Magnetic Frustration

A close inspection of the colors in Fig. 2 reveals a subtle point. Whereas the T_C and Θ_W values are nearly identical at the left corner of the phase diagram, they are quite different at the right corner. This observation implies the presence of a moderate magnetic frustration in the compositions near CrCl_3 . To clarify, we construct a triangular phase diagram of the frustration index, $f = \Theta_W/T_C$, in Fig. 4. A large frustration index indicates a small T_C relative to the

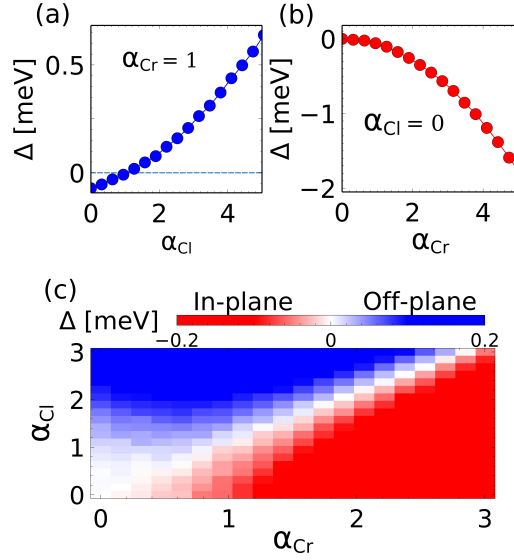


Figure 5: (a) The magnetic anisotropy energy Δ plotted as a function of Cl SOC (α_{Cl}) by fixing the SOC of Cr to unity ($\alpha_{Cr} = 1$). (b) Δ plotted as a function of the Cr SOC by switching off the Cl SOC ($\alpha_{Cl} = 0$). (c) The anisotropy energy as a function of the SOC in Cr and Cl, showing a competition between in-plane and out-of-plane anisotropies tuned by α_{Cr} and α_{Cl} .

interaction strength $J \propto \Theta_W$ (19). Figure 4 shows that the magnetic frustration is large near CrCl_3 , maximizes at the composition $\text{CrCl}_{2.55}\text{Br}_{0.45}$, and gradually disappears toward either CrBr_3 or CrI_3 . Recent theoretical and experimental works have suggested that CrI_3 could be a frustrated VdW material due to the Kitaev interaction (11, 12). However, Fig. 4 suggests that compositions near CrCl_3 , specifically $\text{CrCl}_{2.55}\text{Br}_{0.45}$, are more promising to look for the frustration effects. This is consistent with the competition scenario between the SOC of the transition-metal and ligand (or equivalently, between D and λ in Eq. 1), because the atomic SOC in Cr (90 meV) is comparable to Cl (40 meV), but much smaller than Br (220 meV) and I (580 meV).

Density Functional Theory

The competition scenario in Eq. 1 and the resulting magnetic frustration in Fig. 4 can be demonstrated from first-principles. We performed DFT calculations for the pure CrCl_3 by controlling the strength of the SOC contributions from Cr and Cl individually. The DFT Hamiltonian can

be written as (9)

$$\mathcal{H}_{DFT} = \mathcal{H}_0 + \alpha_{Cr}\mathcal{H}_{SOC}^{Cr} + \alpha_{Cl}\mathcal{H}_{SOC}^{Cl} \quad (2)$$

where \mathcal{H}_0 is the non-relativistic Hamiltonian in the absence of any SOC ($\alpha_{Cr} = \alpha_{Cl} = 0$). \mathcal{H}_{SOC}^{Cr} is the SOC correction in Cr and \mathcal{H}_{SOC}^{Cl} is the SOC correction in Cl. By definition, the physical scenario in CrCl_3 corresponds to $\alpha_{Cr} = \alpha_{Cl} = 1$, consistent with the atomic values of the SOC mentioned earlier (15). We can effectively tune the \mathcal{H}_{DFT} from CrCl_3 to CrBr_3 and CrI_3 by increasing α_{Cl} .

Partitioning the Hamiltonian in Eq. 2 enables us to independently control the contribution from Cr and the halide (Cl, Br, I) to the magnetic anisotropy and trace the easy-plane versus easy-axis anisotropy. The anisotropy energy of the system is defined as $\Delta = E_{\rightarrow} - E_{\uparrow}$, where E_{\rightarrow} and E_{\uparrow} are the total DFT energies of the in-plane and out-of-plane FM states, respectively. Thus, a negative (positive) Δ corresponds to easy-plane (easy-axis). In the following, we present the analysis in two steps.

First, we show the evolution of the anisotropy energy as a function of the halide SOC in Fig. 5(a) by fixing the Cr SOC to $\alpha_{Cr} = 1$. With increasing α_{Cl} , Δ gradually approaches zero from negative and turns positive, i.e. the in-plane anisotropy is gradually replaced by out-of-plane anisotropy. In CrCl_3 , where $\alpha_{Cr} = \alpha_{Cl} = 1$, the system conserves its easy-plane anisotropy, in agreement with the experimental observation. The alloying process effectively increases the ligand SOC ($\alpha_{Cl} > 1$) and leads to $\Delta > 0$, corresponding to the out-of-plane anisotropy found in CrBr_3 and CrI_3 .

Second, we show in Fig. 5(b) the evolution of the anisotropy as a function of α_{Cr} by switching off the SOC of Cl ($\alpha_{Cl} = 0$). We observe a growing tendency toward in-plane anisotropy (negative Δ) by increasing the Cr SOC. This result confirms that the Cr SOC favors in-plane anisotropy and competes with the halide SOC.

The generic competition between the SOC of the magnetic atom (Cr) and the ligand (Cl) is mapped in Fig. 5(c), showing that the anisotropy direction is controlled by the relative strength of the two SOC constants, α_{Cr} and α_{Cl} . Notice that CrCl_3 is on the borderline between the

in-plane and out-of-plane anisotropy. Thus, the D and λ terms in Eq. 1 nearly cancel each other and drive CrCl_3 toward a frustrated regime (Fig. 4). In contrast, the strong ligand SOC in CrBr_3 and CrI_3 induces a robust out-of-plane FM order and relieves the magnetic frustration. In other words, $H_{\text{frust.}}$ becomes perturbatively irrelevant at low energies in Eq. 1 when the system has a robust easy-axis. We point out that a bare DFT calculation could erroneously predict an easy-axis, instead of easy-plane, in CrCl_3 (20). We had to implement a small (2%) lattice compression to match the DFT results with the experimental in-plane anisotropy in CrCl_3 (details in the SM). We also present DFT results for CrBr_3 in the SM that correctly confirm out-of-plane anisotropy.

Metamagnetic Transition

The first important finding in our experiments was a frustrated regime near CrCl_3 where the effects of D and λ in Eq. 1 nearly cancel out, allowing $H_{\text{frust.}}$ to show its effect. Our second exciting finding is that the inter-layer magnetic coupling in the VdW alloys is different from the parent compounds. Recently, a metamagnetic (MM) transition has been reported at 0.7 T in the bilayers of CrI_3 due to a field-induced change of interlayer coupling from AF to FM (4, 5). The AF-FM switching of the inter-layer coupling produces a sharp step in the $M(H)$ curves of CrI_3 bilayers, corresponding to a spin-flop transition. This effect has been utilized in a spin-filter magnetic tunnel junction where a step-like magnetoresistance has been observed at the MM transition (21, 22). Figure 6(a) shows a similar MM transition in the bulk crystals of $\text{CrCl}_{0.8}\text{Br}_{1.2}\text{I}_{1.0}$ as a function of field. Notice that the transition is observed only when the field is perpendicular to the plane (B_{\perp}). A magnified view of the $M(B)$ curves in Fig. 6(b) shows that the transition occurs at $B_{\perp} = 0.7$ T, the same field at which CrI_3 bilayers undergo a spin-flip transition (4, 5). However, the MM transition in $\text{CrCl}_{0.8}\text{Br}_{1.2}\text{I}_{1.0}$ is less sharp than in the bilayers of CrI_3 (4). As such, we assign this transition to a field-induced spin-canting, instead of spin-flop, as illustrated in the inset of Fig. 6(b).

Chemical inhomogeneity or disorder do not play a role in either the MM transition or mag-

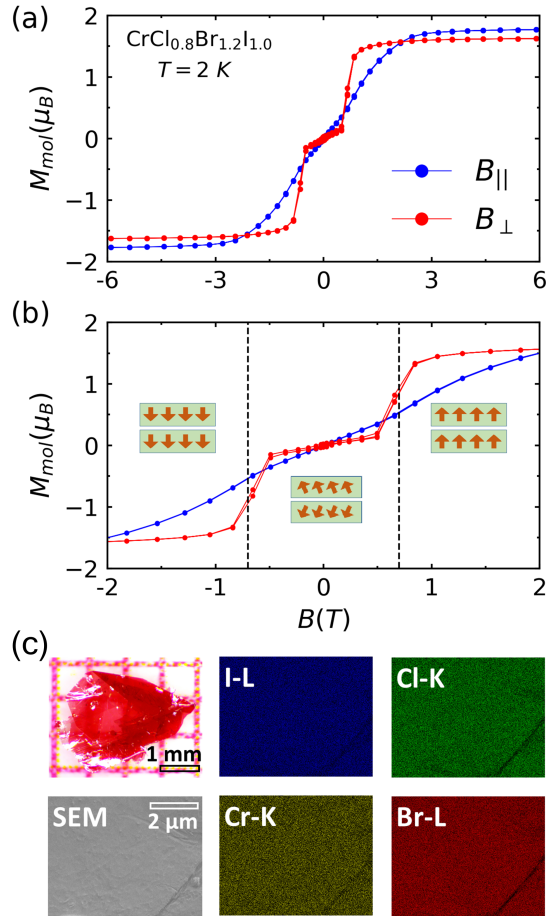


Figure 6: (a) Magnetization plotted as a function of field in $\text{CrCl}_{0.8}\text{Br}_{1.2}\text{I}_{1.0}$. The red and blue data correspond to the field perpendicular (B_{\perp}) and parallel (B_{\parallel}) to the honeycomb layers, respectively. The saturated moment is consistent with $S = 3/2$ in Cr^{3+} . (b) Magnified view of the spin-canting transition at $B_{\perp} = 0.7\text{ T}$. (c) Optical image, SEM image, and EDX color maps reveal a uniform distribution of Cr (yellow, K -edge), Cl (green, K -edge), Br (red, L -edge), and I (blue, L -edge) in $\text{CrCl}_{0.8}\text{Br}_{1.2}\text{I}_{1.0}$.

netic frustration. We performed energy-dispersive X-ray spectroscopy (EDX) on each sample inside a scanning electron microscope (SEM). The SEM-EDX color maps in Fig. 6(c) confirm a uniform distribution of Cr, Cl, Br, and I atoms in a $\text{CrCl}_{0.8}\text{Br}_{1.2}\text{I}_{1.0}$ crystal and rule out a phase separation scenario. In materials with impurity phases or inhomogeneous distribution of elements, the color maps reveal regions of dark and light shade (23). A table of EDX results is reported in the SM. Furthermore, all three-halide VdW alloys show a single sharp magnetic transition (Figs. 3, S2, and S3), similar to the parent compounds (24). If the samples were disordered or chemically inhomogeneous, we would have expected either a rounded transition or multiple transitions, which is clearly not the case.

Summary and Outlook

Despite the conventional wisdom to tune magnetism by doping on the cation site where the magnetic moment resides (25, 26), we highlight the remarkable effect of mixing the anions to synthesize a continuum of VdW magnets with chemical control over the ligand SOC. Note that the change of SOC from Cl to I is enormous (more than one order of magnitude) based on the atomic values of SOC (15), whereas the change of local geometry and bond angle is minimal. For example, the Cr-ligand-Cr bond angles are 93.9° and 93.3° in the low-temperature structure of CrCl_3 and CrI_3 , respectively (14, 27). Thus, the dominant tuning parameter in our phase diagrams is the ligand SOC.

The chromium trihalides provided a unique opportunity for our experiments due to their remarkable chemical tunability. Because the SOC of $\text{Cl} < \text{Cr} < \text{Br} < \text{I}$, we were able to tune the SOC of the magnetic ion and the ligands against each other. Without making a solid-solution of three halides and mapping the phase diagram of $\text{CrCl}_{3-x-y}\text{Br}_x\text{I}_y$, it would have been impossible to find the frustrated regime and the change of inter-layer coupling.

We point out that the alloying process inevitably leads to bond randomness. Based on the remarkable agreement between our mean-field DFT approach and the experimental results, it

appears that the bond randomness at an atomic level does not affect the magnetic anisotropy and ordering dramatically. However, it would be an interesting future direction to go beyond the mean-field level and explore the role of bond randomness in VdW alloys near the Kitaev limit (28).

The methods presented here can, in principle, be extended to chalcogenides. Examples of chalcogen-based VdW magnets are the itinerant ferromagnet Fe_3GeTe_2 (29, 30), the FM insulator $\text{Cr}_2\text{Ge}_2\text{Te}_6$ (6), and the AFM layered compound FePS_3 (31, 32). One advantage of the chalcogenides is their relatively high transition temperatures. For example, $T_C = 220$ K in Fe_3GeTe_2 (33), $T_C = 60$ K in $\text{Cr}_2\text{Ge}_2\text{Te}_6$ (34), and $T_N = 118$ K in FePS_3 (31). The magnetic properties of these materials can be controlled by mixing the chalcogens S, Se, and Te. Such efforts will expand the list of desirable VdW magnets (8, 35). But more importantly, they will lead to new regimes (such as frustration) and new phenomena (such as spin-canting transition).

As mentioned earlier, the magnetic ordering in CrI_3 is known to acquire a layer-dependent structure in the atomically thin limit (single layer, bilayer, and trilayer) (5, 17, 22, 36–38). An important question is whether the MM transition at 0.7 T in the bulk crystals of $\text{CrCl}_{0.8}\text{Br}_{1.2}\text{I}_{1.0}$ is due to a change of stacking sequence or a structural transition at low temperatures. This question could be answered by low-temperature synchrotron X-ray experiments in the future.

In the SM, we show that the alloyed crystals are as exfoliable as their parent structures. It will be interesting to exfoliate the bulk crystals of $\text{CrCl}_{0.8}\text{Br}_{1.2}\text{I}_{1.0}$ and isolate bilayers and trilayers to look for a richer pattern of MM transitions by measuring the magneto-optical Kerr Effect (MOKE). Such heterostructures will be an invaluable resource for new devices, such as spin-filter tunneling junctions (21, 22, 39, 40) and magnon-assisted tunneling devices (41).

Materials and Methods

Crystal Growth

The crystals of $\text{CrCl}_{3-x-y}\text{Br}_x\text{I}_y$ were grown by the CVT method from CrCl_3 , CrBr_3 , and CrI_3 precursors mixed with appropriate mole ratios (see Table S1 in the SM). In a typical CVT cycle, 400 mg of the starting mixture was placed inside a 6''-long fused silica tube and held at 650 °C, with a 200 °C temperature gradient, for 72 h. CrCl_3 crystals were grown by vacuum sublimation of polycrystalline CrCl_3 at 650 °C for 72 h. CrBr_3 crystals were grown by annealing a mixture of $\text{Cr}+0.75\text{TeBr}_4$ at 700 °C for 72 h. CrI_3 crystals were grown by annealing a mixture $\text{Cr}+1.5\text{I}_2$ at 650 °C for 72 h. The starting chemicals, Cr(99.99%), CrCl_3 (99.9%), TeBr_4 (99.9%), and I_2 (99.8%) were purchased from Alfa Aesar. The crystals grew in the form of thin plates, several millimeters across and less than 1 μm thick.

Electron Microscopy

The morphology and chemical composition of crystals were studied by scanning electron microscopy (SEM) and energy dispersive X-ray spectroscopy (EDX), using a JEOL 7900F field-emission scanning electron microscope (FESEM) equipped with an EDAX detector.

Magnetic Measurements

Magnetic measurements were performed using a vibrating sample magnetometer (VSM) inside a Quantum Design MPMS-3. Thin plate-like crystals were mounted on a low-background quartz or sapphire holder for the B_{\parallel} and B_{\perp} measurements, respectively.

Density Functional Theory

Density functional theory (DFT) calculations were performed using the all-electron Elk code (42). Lattice relaxations were performed with Quantum Espresso (43), PBEsol functional, and PAW pseudopotentials. A 2% lattice compression was imposed to match the DFT results with the

experimental observations (see SM for details) (20, 44). The total energy convergence was set to $0.027 \mu\text{eV}$ to account for the small energy differences involved in magnetic anisotropies.

References

1. H.-B. Luo, H.-B. Zhang, J. P. Liu, Strong hopping induced Dzyaloshinskii-Moriya interaction and skyrmions in elemental cobalt. *npj Computational Materials* **5**, 1–6 (2019). Number: 1 Publisher: Nature Publishing Group.
2. H. Takagi, T. Takayama, G. Jackeli, G. Khaliullin, S. E. Nagler, Concept and realization of Kitaev quantum spin liquids. *Nature Reviews Physics* **1**, 264–280 (2019). Number: 4 Publisher: Nature Publishing Group.
3. F. Bahrami, W. Lafargue-Dit-Hauret, O. I. Lebedev, R. Movshovich, H.-Y. Yang, D. Broido, X. Rocquefelte, F. Tafti, Thermodynamic Evidence of Proximity to a Kitaev Spin Liquid in $\text{Ag}_3\text{LiIr}_2\text{O}_6$. *Physical Review Letters* **123**, 237203 (2019). Publisher: American Physical Society.
4. B. Huang, G. Clark, E. Navarro-Moratalla, D. R. Klein, R. Cheng, K. L. Seyler, D. Zhong, E. Schmidgall, M. A. McGuire, D. H. Cobden, W. Yao, D. Xiao, P. Jarillo-Herrero, X. Xu, Layer-dependent ferromagnetism in a van der Waals crystal down to the monolayer limit. *Nature* **546**, 270–273 (2017).
5. S. Jiang, L. Li, Z. Wang, K. F. Mak, J. Shan, Controlling magnetism in 2D CrI_3 by electrostatic doping. *Nature Nanotechnology* **13**, 549–553 (2018).
6. C. Gong, L. Li, Z. Li, H. Ji, A. Stern, Y. Xia, T. Cao, W. Bao, C. Wang, Y. Wang, Z. Q. Qiu, R. J. Cava, S. G. Louie, J. Xia, X. Zhang, Discovery of intrinsic ferromagnetism in two-dimensional van der Waals crystals. *Nature* **546**, 265–269 (2017).

7. N. D. Mermin, H. Wagner, Absence of Ferromagnetism or Antiferromagnetism in One- or Two-Dimensional Isotropic Heisenberg Models. *Physical Review Letters* **17**, 1133–1136 (1966). Publisher: American Physical Society.
8. K. S. Burch, D. Mandrus, J.-G. Park, Magnetism in two-dimensional van der Waals materials. *Nature* **563**, 47–52 (2018).
9. J. L. Lado, J. Fernandez-Rossier, On the origin of magnetic anisotropy in two dimensional CrI₃. *2D Materials* **4**, 035002 (2017).
10. D. Torelli, T. Olsen, Calculating critical temperatures for ferromagnetic order in two-dimensional materials. *2D Materials* **6**, 015028 (2018).
11. C. Xu, J. Feng, H. Xiang, L. Bellaiche, Interplay between Kitaev interaction and single ion anisotropy in ferromagnetic CrI₃ and CrGeTe₃ monolayers. *npj Computational Materials* **4**, 1–6 (2018).
12. I. Lee, F. G. Utermohlen, D. Weber, K. Hwang, C. Zhang, J. van Tol, J. E. Goldberger, N. Trivedi, P. C. Hammel, Fundamental Spin Interactions Underlying the Magnetic Anisotropy in the Kitaev Ferromagnet CrI₃. *Physical Review Letters* **124**, 017201 (2020).
13. J. W. Cable, M. K. Wilkinson, E. O. Wollan, Neutron diffraction investigation of antiferromagnetism in CrCl₃. *Journal of Physics and Chemistry of Solids* **19**, 29–34 (1961).
14. M. A. McGuire, H. Dixit, V. R. Cooper, B. C. Sales, Coupling of Crystal Structure and Magnetism in the Layered, Ferromagnetic Insulator CrI₃. *Chemistry of Materials* **27**, 612–620 (2015).
15. W. C. Martin, *Table of spin-orbit energies for p-electrons in neutral atomic (core) np configurations* (National Bureau of Standards, 1971).
16. T. Li, S. Jiang, N. Sivadas, Z. Wang, Y. Xu, D. Weber, J. E. Goldberger, K. Watanabe, T. Taniguchi, C. J. Fennie, K. Fai Mak, J. Shan, Pressure-controlled interlayer magnetism

- in atomically thin CrI₃. *Nature Materials* **18**, 1303–1308 (2019). Number: 12 Publisher: Nature Publishing Group.
17. W. Chen, Z. Sun, Z. Wang, L. Gu, X. Xu, S. Wu, C. Gao, Direct observation of van der Waals stackingdependent interlayer magnetism. *Science* **366**, 983–987 (2019).
 18. M. Abramchuk, S. Jaszewski, K. R. Metz, G. B. Osterhoudt, Y. Wang, K. S. Burch, F. Tafti, Controlling Magnetic and Optical Properties of the van der Waals Crystal CrCl_{3-x}Br_x via Mixed Halide Chemistry. *Advanced Materials* **30**, 1801325 (2018).
 19. A. P. Ramirez, Strongly Geometrically Frustrated Magnets. *Annual Review of Materials Science* **24**, 453–480 (1994).
 20. L. Webster, J.-A. Yan, Strain-tunable magnetic anisotropy in monolayer CrCl₃, CrBr₃, and CrI₃. *Physical Review B* **98**, 144411 (2018).
 21. T. Song, X. Cai, M. W.-Y. Tu, X. Zhang, B. Huang, N. P. Wilson, K. L. Seyler, L. Zhu, T. Taniguchi, K. Watanabe, M. A. McGuire, D. H. Cobden, D. Xiao, W. Yao, X. Xu, Giant tunneling magnetoresistance in spin-filter van der Waals heterostructures. *Science* **360**, 1214–1218 (2018).
 22. D. R. Klein, D. MacNeill, J. L. Lado, D. Soriano, E. Navarro-Moratalla, K. Watanabe, T. Taniguchi, S. Manni, P. Canfield, J. Fernandez-Rossier, P. Jarillo-Herrero, Probing magnetism in 2d van der Waals crystalline insulators via electron tunneling. *Science* **360**, 1218–1222 (2018).
 23. M. Abramchuk, T. Mier, F. Tafti, Tuning the magnetic and structural properties of a three-metal boride alloy: Mn_{0.95-δ}Fe_{1.05+δ-x}Co_xB. *Journal of Alloys and Compounds* **805**, 909–914 (2019).
 24. M. A. McGuire, Crystal and Magnetic Structures in Layered, Transition Metal Dihalides and Trihalides. *Crystals* **7**, 121 (2017).

25. C. Bi, S. Wang, W. Wen, J. Yuan, G. Cao, J. Tian, Room-Temperature Construction of Mixed-Halide Perovskite Quantum Dots with High Photoluminescence Quantum Yield. *The Journal of Physical Chemistry C* **122**, 5151–5160 (2018).
26. H. F. Zarick, N. Soetan, W. R. Erwin, R. Bardhan, Mixed halide hybrid perovskites: a paradigm shift in photovoltaics. *Journal of Materials Chemistry A* **6**, 5507–5537 (2018).
27. B. Morosin, A. Narath, XRay Diffraction and Nuclear Quadrupole Resonance Studies of Chromium Trichloride. *The Journal of Chemical Physics* **40**, 1958–1967 (1964). Publisher: American Institute of Physics.
28. J. Knolle, R. Moessner, N. B. Perkins, Bond-Disordered Spin Liquid and the Honeycomb Iridate $\text{H}_3\text{LiIr}_2\text{O}_6$: Abundant Low-Energy Density of States from Random Majorana Hopping. *Physical Review Letters* **122**, 047202 (2019). Publisher: American Physical Society.
29. Z. Fei, B. Huang, P. Malinowski, W. Wang, T. Song, J. Sanchez, W. Yao, D. Xiao, X. Zhu, A. F. May, W. Wu, D. H. Cobden, J.-H. Chu, X. Xu, Two-dimensional itinerant ferromagnetism in atomically thin Fe_3GeTe_2 . *Nature Materials* **17**, 778–782 (2018).
30. Y. Deng, Y. Yu, Y. Song, J. Zhang, N. Z. Wang, Z. Sun, Y. Yi, Y. Z. Wu, S. Wu, J. Zhu, J. Wang, X. H. Chen, Y. Zhang, Gate-tunable room-temperature ferromagnetism in two-dimensional Fe_3GeTe_2 . *Nature* **563**, 94–99 (2018).
31. J.-U. Lee, S. Lee, J. H. Ryoo, S. Kang, T. Y. Kim, P. Kim, C.-H. Park, J.-G. Park, H. Cheong, Ising-Type Magnetic Ordering in Atomically Thin FePS_3 . *Nano Letters* **16**, 7433–7438 (2016).
32. X. Wang, K. Du, Y. Y. F. Liu, P. Hu, J. Zhang, Q. Zhang, M. H. S. Owen, X. Lu, C. K. Gan, P. Sengupta, C. Kloc, Q. Xiong, Raman spectroscopy of atomically thin two-dimensional magnetic iron phosphorus trisulfide (FePS_3) crystals. *2D Materials* **3**, 031009 (2016).

33. K. Kim, J. Seo, E. Lee, K.-T. Ko, B. S. Kim, B. G. Jang, J. M. Ok, J. Lee, Y. J. Jo, W. Kang, J. H. Shim, C. Kim, H. W. Yeom, B. Il Min, B.-J. Yang, J. S. Kim, Large anomalous Hall current induced by topological nodal lines in a ferromagnetic van der Waals semimetal. *Nature Materials* **17**, 794–799 (2018).
34. H. Ji, R. A. Stokes, L. D. Alegria, E. C. Blomberg, M. A. Tanatar, A. Reijnders, L. M. Schoop, T. Liang, R. Prozorov, K. S. Burch, N. P. Ong, J. R. Petta, R. J. Cava, A ferromagnetic insulating substrate for the epitaxial growth of topological insulators. *Journal of Applied Physics* **114**, 114907 (2013).
35. C. Gong, X. Zhang, Two-dimensional magnetic crystals and emergent heterostructure devices. *Science* **363** (2019).
36. B. Huang, G. Clark, D. R. Klein, D. MacNeill, E. Navarro-Moratalla, K. L. Seyler, N. Wilson, M. A. McGuire, D. H. Cobden, D. Xiao, W. Yao, P. Jarillo-Herrero, X. Xu, Electrical control of 2d magnetism in bilayer CrI₃. *Nature Nanotechnology* **13**, 544–548 (2018).
37. Z. Wang, T. Zhang, M. Ding, B. Dong, Y. Li, M. Chen, X. Li, J. Huang, H. Wang, X. Zhao, Y. Li, D. Li, C. Jia, L. Sun, H. Guo, Y. Ye, D. Sun, Y. Chen, T. Yang, J. Zhang, S. Ono, Z. Han, Z. Zhang, Electric-field control of magnetism in a few-layered van der Waals ferromagnetic semiconductor. *Nature Nanotechnology* **13**, 554–559 (2018).
38. K. L. Seyler, D. Zhong, D. R. Klein, S. Gao, X. Zhang, B. Huang, E. Navarro-Moratalla, L. Yang, D. H. Cobden, M. A. McGuire, W. Yao, D. Xiao, P. Jarillo-Herrero, X. Xu, Ligand-field helical luminescence in a 2d ferromagnetic insulator. *Nature Physics* **14**, 277–281 (2018).
39. Z. Wang, I. Gutierrez-Lezama, N. Ubrig, M. Kroner, M. Gibertini, T. Taniguchi, K. Watanabe, A. Imamolu, E. Giannini, A. F. Morpurgo, Very large tunneling magnetoresistance in layered magnetic semiconductor CrI₃. *Nature Communications* **9**, 1–8 (2018).

40. H. H. Kim, B. Yang, T. Patel, F. Sfigakis, C. Li, S. Tian, H. Lei, A. W. Tsen, One Million Percent Tunnel Magnetoresistance in a Magnetic van der Waals Heterostructure. *Nano Letters* **18**, 4885–4890 (2018).
41. D. Ghazaryan, M. T. Greenaway, Z. Wang, V. H. Guarochico-Moreira, I. J. Vera-Marun, J. Yin, Y. Liao, S. V. Morozov, O. Kristanovski, A. I. Lichtenstein, M. I. Katsnelson, F. Withers, A. Mishchenko, L. Eaves, A. K. Geim, K. S. Novoselov, A. Misra, Magnon-assisted tunnelling in van der Waals heterostructures based on CrBr₃. *Nature Electronics* **1**, 344–349 (2018).
42. The Elk Code, <http://elk.sourceforge.net> (2019).
43. P. Giannozzi, S. Baroni, N. Bonini, M. Calandra, R. Car, C. Cavazzoni, D. Ceresoli, G. L. Chiarotti, M. Cococcioni, I. Dabo, A. D. Corso, S. d. Gironcoli, S. Fabris, G. Fratesi, R. Gebauer, U. Gerstmann, C. Gougoussis, A. Kokalj, M. Lazzeri, L. Martin-Samos, N. Marzari, F. Mauri, R. Mazzarello, S. Paolini, A. Pasquarello, L. Paulatto, C. Sbraccia, S. Scandolo, G. Sclauzero, A. P. Seitsonen, A. Smogunov, P. Umari, R. M. Wentzcovitch, QUANTUM ESPRESSO: a modular and open-source software project for quantum simulations of materials. *Journal of Physics: Condensed Matter* **21**, 395502 (2009).
44. P. Bruno, Spin-wave theory of two-dimensional ferromagnets in the presence of dipolar interactions and magnetocrystalline anisotropy. *Physical Review B* **43**, 6015–6021 (1991).

Acknowledgements: F.T. acknowledges support from the National Science Foundation under Grant No. DMR-1708929. J.Y.C acknowledges support from the National Science Foundation under Grant No. DMR-1700030. Y.R. acknowledges support from the National Science Foundation under Grant No. DMR-1712128. J.L.L. acknowledges the computational resources provided by the Aalto Science-IT project. M.D and K.S.B. acknowledge support from the US Department of Energy (DOE), Office of Science, Office of Basic Energy Sciences under award no. de-sc0018675.

Author Contributions: TT, JNT, and MA grew the crystals and performed measurements. TT, JNT, and FB analyzed data. JLL performed DFT calculations. GTM and JYC characterized the samples. MD and KSB performed exfoliation. All authors contributed to writing the manuscript. YR and FT initiated the project.

Competing Interests: The authors declare that they have no competing financial interests.

Data and materials availability: Additional data and materials are available online.

Supplementary Material: This paper has supplementary material in a separate PDF file.